RESEARCH ARTICLE

Journal of Medical Imaging and Health Informatics
Vol. 4, 1–9, 2014

An Intrinsic Image Representation and Its Application to Left Ventricle Segmentation in Cardiac MRI Images

Hyo-Hoon Kim, Poltayev Rassulzhan, and Byung-Woo Hong*

Computer Science Department, Chung-Ang University, Seoul, Korea

In this work, we presents an interactive image segmentation algorithm based on the extraction of isocontours at specified points from an intrinsic image representation that is obtained by our image decomposition algorithm. Our image decomposition is designed to remove undesirable bias field and noise from a variety of medical images in a variational framework and our segmentation is developed using isocontours obtained by a marching cube algorithm via interactive selection of initial points of the contours on the intrinsic image where the effect of undesirable bias field and noise are reduced. The experimental results demonstrate the robustness and effectiveness of our algorithm in the delineation of left ventricles in cardiac MRI images, and show a potential as the basis for an image annotation tool in the diagnosis or treatment procedure based on medical images.

Keywords: Cardiac MRI, Left Ventricle Segmentation, Image Decomposition, Marching Cubes, Total Variation.

1. INTRODUCTION

Image segmentation plays a significant role in understanding medical images. This critical task involves partitioning an image domain into sub-domains based on a statistical homogeneity criterion. In particular, anatomical or functional analysis of organs or structures plays an important role in the diagnosis of diseases. However, it is considered as a difficult problem due to undesirable noises and biased illumination artifacts which are generally involved in the image formation process for a variety of imaging modalities such as MRI. Thus, image segmentation still remains as a challenging problem even though there have been a large number of algorithms to tackle this problem. Image segmentation is generally performed based on the homogeneity of intensities for region-based approaches or the strength of the edgeness for edge-based approaches. In often cases the assumption that is associated with the segmentation algorithm is violated due to the introduction of undesirable noises or uneven illuminations. This indicates that the image representation is tightly related to the performance of the segmentation algorithm. This observation is also true for the analysis of medical imagery. Among a variety of applications in medical imaging, the functional and anatomical analysis of heart in cardiac MRI is considered as one of the most significant tasks. The analysis procedure may include the computation of heart volume, wall thickness, blood flows, and the cardiac motion. There properties are considered as significant in the diagnosis of heart disease that may causes syncope and sudden cardiac death.[1–3] In this work, we propose an interactive segmentation algorithm developed in a structural approach that implicitly combines the advantages of both local and global features. The topological and geometrical properties of image structures are analyzed by the extraction of isocontours that characterize salient regions. The saliency is measured in terms of the connectivity of the neighboring pixels and the size of the connected component that is confined by the isocontour. The structural analysis is performed on the intrinsic form of images which is obtained by our image decomposition procedure discarding bias fields and noises. We introduce an image model assuming that the observation consists of the addition of the intrinsic component and undesirable noise and bias field. The image decomposition algorithm is developed based on Total Variation technique[4] to decompose the observation into its intrinsic component and other undesirable nuisance components in a variational framework. A simple marching cube algorithm[5] is applied to define the boundary of left ventricle based on the obtained intrinsic representation from a manually selected point in an interactive way. The performance of the algorithm is quantitatively evaluated in the problem of left ventricle segmentation in cardiac MRI.

2. LITERATURE REVIEW

There have been a large number of cardiac region segmentation algorithms that can be categorized into boundary-based

*Author to whom correspondence should be addressed.

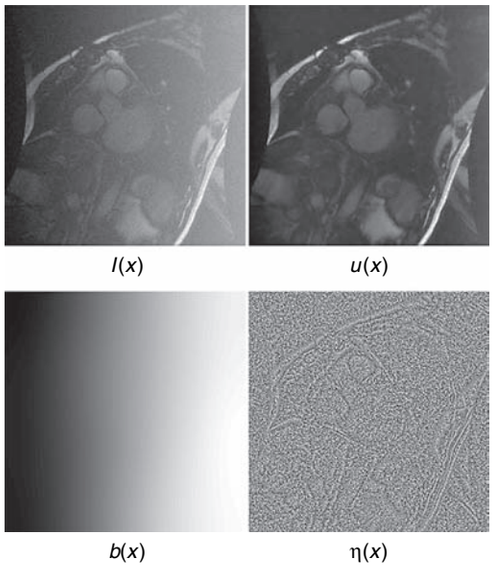

Fig. 1. An example of cardiac MRI image $I(x)$ and its decomposition into the intrinsic image $u(x)$, bias field $b(x)$, and noise $n(x)$.

or region-based approach in a discrete or continuous setting.[6] Boundary driven approaches include active contour and geodesic active contour.[3, 7–9] Active contour models have been used to estimate the boundary of endocardium, myocardium, and epicardium in the level set framework.[10] Even though the numerical efficiency of the level set method, the active contour techniques requires user-specified initialization and often shape priors to overcome the subtle image features.[11, 12] There has been an approach for an automatic segmentation for the left ventricle based on a deformable model,[13] however the algorithm suffers from noise and heterogeneity of the cardiac MRI image. Boundary driven left ventricle segmentation algorithms use an energy functional that consists of strength of edgeness and regularization to find structure of left ventricle with distinctive edges. However, these methods are known to be sensitive to noise.[14, 15] The computation of the image gradient involves derivative operations that magnify undesirable noises. A region-based approach has been introduced to overcome the sensitivity with respect to noise based on Mumford-Shah functional that consists of data fitting term and regularization term.[16–18] However, these algorithms are computationally expensive. As a simple algorithm in a discrete setting, Watershed algorithm has been introduced to detect blob-like regions.[19–21] The algorithm has been applied to separate left ventricle from surrounding organs in MRI.[22] As an alternative approach, clustering techniques are introduced to yield partitions of image domain, which is performed based on the similarity of intensity properties. Clustering algorithm can split the left ventricle and the other structures in the cardiac region automatically.[23, 24] But these methods need to specify the region of interest to exclude undesired objects while clustering is performed. A graph-cut based approach is also considered as one of the most popular algorithms in image segmentation.[25] A graph cut algorithm with manually selected seed points is developed using a global optimization scheme.[26] In cardiac region, seed points can be placed automatically using some prior information such as constraints of smoothness.[27, 28] However, these approaches have to change constraints when the condition of image acquisition changes. It is also known that these methods are sensitive to image quality due to its dependency on the intensity values. It is often required to introduce prior knowledge for segmenting regions whose shapes are known by training phases. Active Appearance Model (AAM) or Active Shape Model (ASM) are well known models for segmentation incorporating appearance or shape priors.[29–33] In the detection of left ventricle in cardiac data, a shape information has been used as a prior knowledge.[30, 34–36]

3. METHODS

3.1. Image Model

We propose an image model to use in following image decomposition process. Let $I: \Omega \subset \mathbb{R}^2 \to \mathbb{R}$ be an image where Ω is the image domain. An observed image $I(x)$ is assumed to consist of the desired true image $u(x)$, the global bias field $b(x)$, and the noise $\eta(x)$ with the additive relations as follows:

$$I = u + b + \eta \tag{1}$$

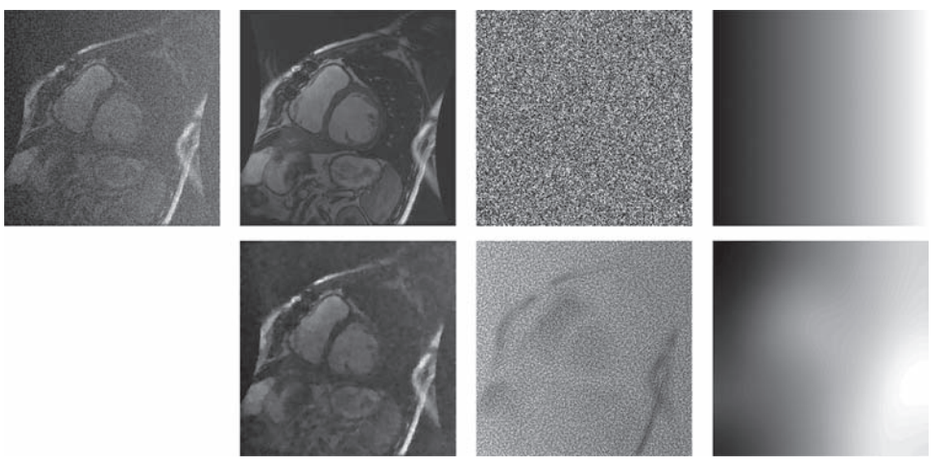

Fig. 2. Visual illustration of the image decomposition result on an example cardiac MRI image with artificial noise and bias field. [Top row] (first) image with noise and bias field, (second) original image, (third) noise, (fourth) bias field. [Bottom row] (second) obtained intrinsic image, (third) estimated noise, (fourth) estimated bias field.

where $u: \Omega \to \mathbb{R}$ is a real-valued function, $b: \Omega \to \mathbb{R}$ is a real-valued function, and $\eta(x) \sim \mathcal{N}(0, \sigma^2)$ is a Gaussian random variable with mean 0 and variance σ^2. The proposed image model is designed to cope with undesirable bias fields that may occur in particular during the imaging procedure of magnetic resonance imaging (MRI). The bias field is a slowly varying low-frequency signal which distorts MRI images, and thus leads to degrade the performance of the image segmentation.[37] As an additional degrading factor, insignificant intensity perturbations are considered as the noise that causes the segmenting boundary to be jagged.[38] An example of our image decomposition is shown in Figure 1. Given an observed image $I(x)$, the intrinsic image component $u(x)$ after removing the bias field $b(x)$ and the noise $\eta(x)$ is desired as a basis where a segmentation procedure is applied. Our image segmentation scheme is based on the isocontour that connects a point set of the same intensity level, and thus the intrinsic image component is preferable to the original image since the intensity of a region in the intrinsic image is directly related to its physical properties which characterize the region boundary. Therefore, the image decomposition is performed as a pre-processing step for segmentation and its computation is discussed in the following section.

3.2. Image Decomposition

The computation of the intrinsic image component from an observed image can be performed in an inverse problem framework using a variational approach. The inverse problem considered in this image decomposition aims to find u from I in Eq. (1)

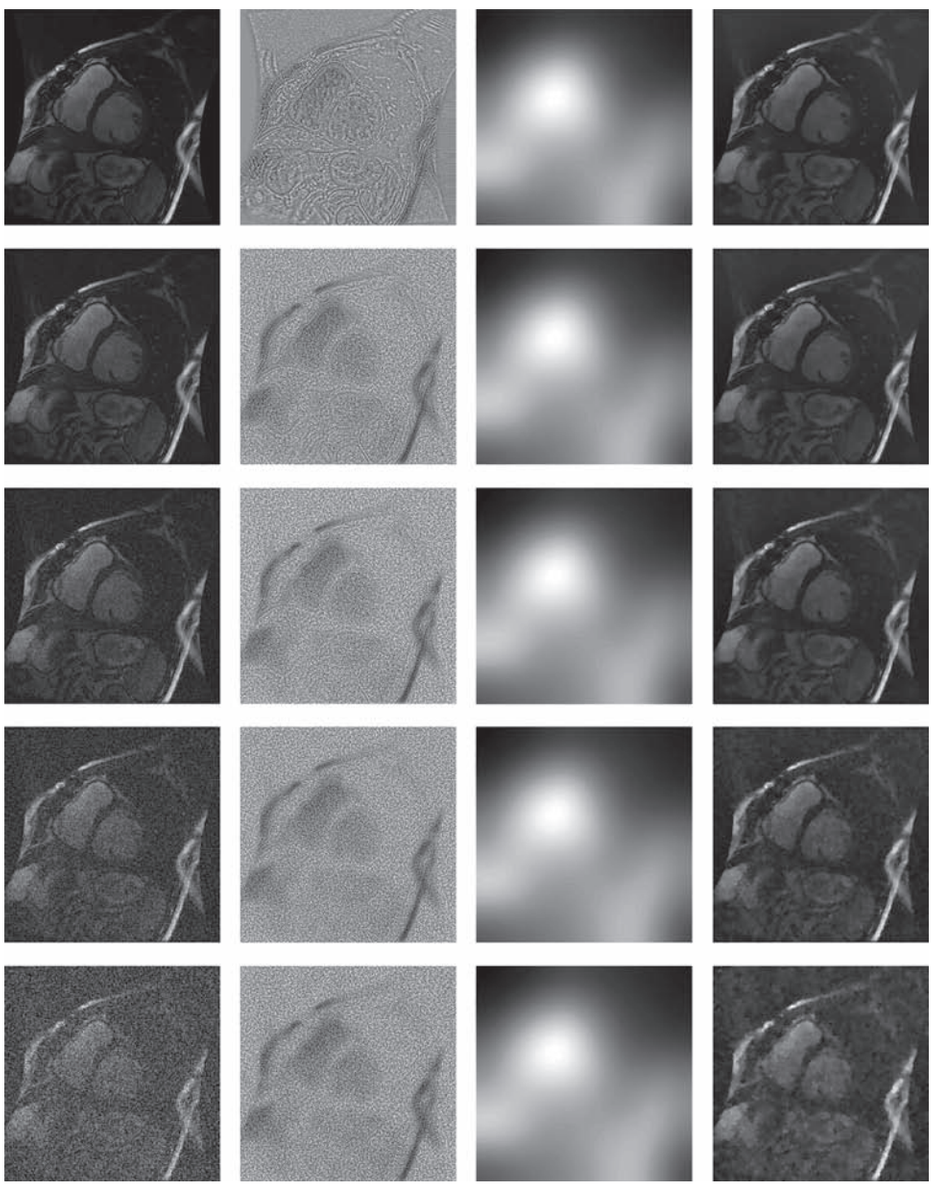

Fig. 3. Visual illustration of the image decomposition results obtained from the images with different levels of noise. [First column] shows the images with artificial Gaussian noise. [Second column] shows the noise component. [Third column] shows the bias field. [Fourth column] shows the intrinsic images.

in which inferring u from measured I is ill-posed. Therefore, it is required to impose constraints on the unknowns in order to make the problem well-defined. We formulate the image decomposition problem in a probabilistic setting using the Bayesian approach. The optimal intrinsic component u and the bias illumination field b are obtained by maximizing the posterior probability $P(u, b \mid I)$ given an observed image I. The posterior probability $P(u, b \mid I)$ can be expressed in terms of the likelihood $P(I \mid u, b)$ and the prior $P(u, b)$ using Bayes' theorem with the assumption of the statistical independence of u and b as follows:

$$P(u, b \mid I) = \frac{P(I \mid u, b)P(u, b)}{P(I)}, \qquad P(u, b \mid I) \propto P(I \mid u, b)P(u)P(b) \tag{2}$$

where $P(I \mid u, b)$ measures how likely the image I is given the knowledge of the states on u and b, and the probabilities $P(u)$ and $P(b)$ encodes the knowledge about the possible states of u and b, respectively. Given the proposed image model in Eq. (1), we derive the likelihood probability based on the Gaussian noise assumption as follows:

$$P(I \mid u, b) \propto \exp\left(-\frac{1}{2{\sigma_1}^2}\int_\Omega (I(x) - u(x) - b(x))^2 \, \mathrm{d}x\right) \tag{3}$$

where σ_1 denotes the standard deviation of the noise. In the modelling of the prior probability $P(u)$, we assume that the gradient of the desired intrinsic image component follows a Laplace distribution leading to the following total variation expression:

$$P(u) \propto \exp\left(-\frac{1}{2\sigma_2}\int_\Omega |\nabla u(x)| \, \mathrm{d}x\right) \tag{4}$$

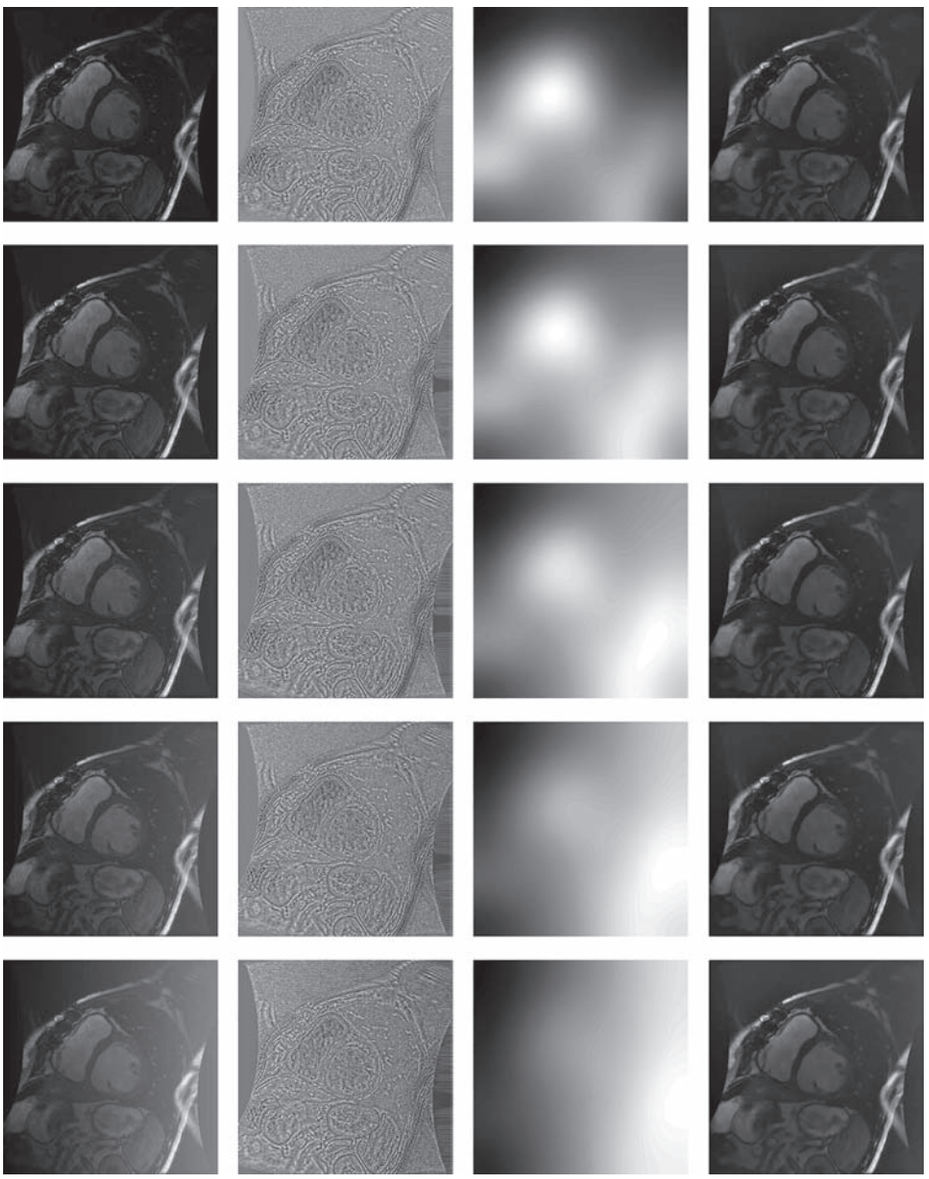

Fig. 4. Visual illustration of the image decomposition results obtained from the images with different levels of bias field. [First column] shows the images with artificial uneven bias fields. [Second column] shows the noise component. [Third column] shows the bias field. [Fourth column] shows the intrinsic images.

where σ_2 is related to the intensity variation within the intrinsic image component u. The total variation regularization is known to be effective in discarding insignificant oscillations while preserving geometric features such as edges or corners.[39] The total variation regularization with respect to the intrinsic image allows our segmentation scheme to implicitly impose the length regularity due to the co-area formula stating that the total variation of a function equals the integral over the length of the boundaries of all its level sets.[40] Our segmentation procedure builds on the isocontour algorithm that draws a simply connected closed curve at locations of same intensity from the intrinsic image and the regularity on the isocontours at every level is implicitly imposed by the total variation regularization. The prior probability on the bias field $P(b)$ is given based on the observation that the bias field forms a smoothly varying intensity field, which can be modelled by a smooth function that tends to have low values for its derivatives. We assume that the partial derivative of the bias field at each point is statistically independent and follows a Gaussian distribution:

$$P(b) \propto \exp\left(-\frac{1}{2\sigma_3{}^2}\int_\Omega |\nabla b(x)|^2\,\mathrm{d}x\right) \tag{5}$$

where σ_3 denotes the standard deviation related to the allowable smoothness within the bias field. The probability $P(b)$ is designed to penalize abrupt changes of the spatial illumination. Given that the likelihood and prior probabilities are defined, we compute the optimal intrinsic image component u^* and the bias field b^* by the maximum a-posteriori (MAP) estimation method as follows:

$$(u^*, b^*) = \underset{(u,b)}{\operatorname{argmax}}\, p(u, b \mid I) = \underset{(u,b)}{\operatorname{argmax}}\, P(I \mid u, b)P(u)P(b) \tag{6}$$

We now define the energy functional $E(u, b; I)$ with respect to u and b given I by taking negative log as follows:

$$\begin{aligned} E(u, b; I) &= -\log(P(I \mid u, b)) - \log(P(u)) - \log(P(b)) \\ &= \int_\Omega (I(x) - u(x) - b(x))^2\,\mathrm{d}x \\ &\quad + \alpha\int_\Omega |\nabla u(x)|\,\mathrm{d}x + \beta\int_\Omega |\nabla b(x)|^2\,\mathrm{d}x \end{aligned} \tag{7}$$

where $\alpha, \beta \in \mathbb{R}$ are the control parameters for the regularization on the intrinsic image and the bias field, respectively. The MAP estimation procedure leads to a minimization problem of

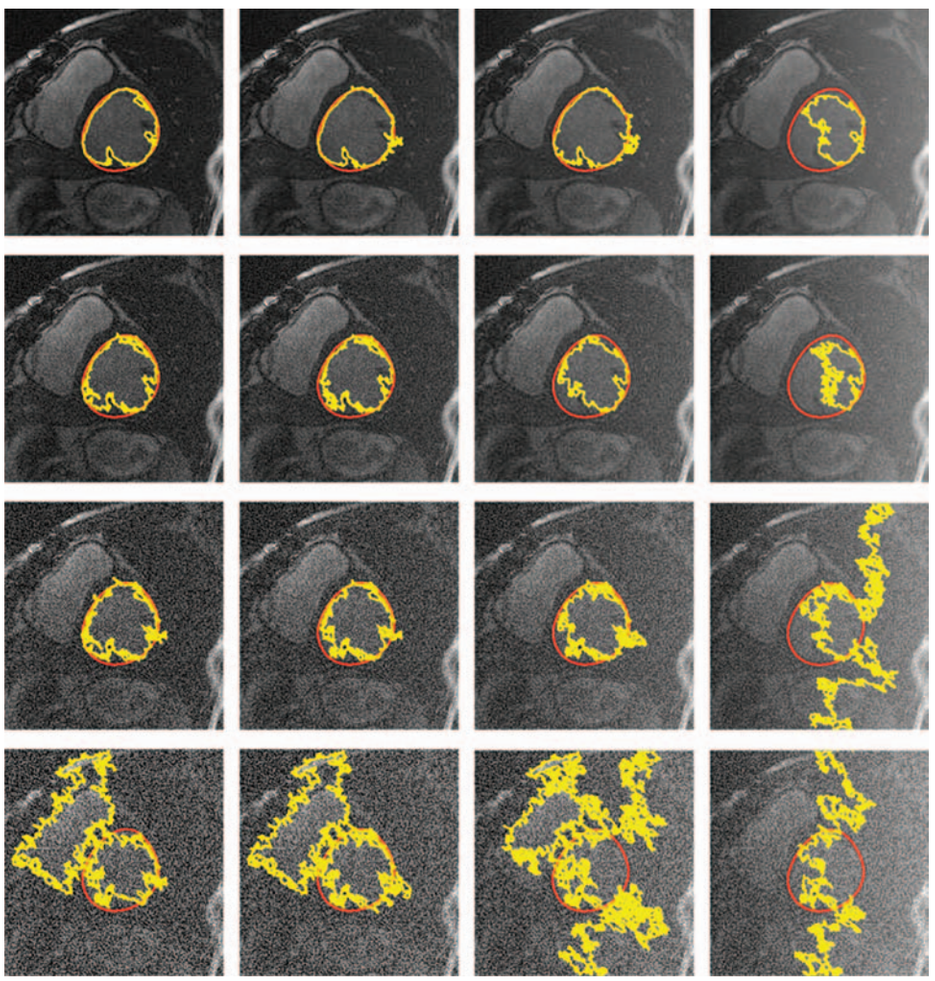

Fig. 5. The segmentation results for the left ventricle obtained from the original images that include artificial noises and bias fields with different levels. The degree of noise is increased from top to bottom and the degree of bias field is increased from left to right. The segmentation results are shown in yellow color and the ground truth is shown in red color.

the energy functional defined in Eq. (7) that can be grouped into two energy components E_1 and E_2 for unknown u and b, respectively as follows:

$$E_1(u; I, b) = \int_\Omega (I(x) - u(x) - b(x))^2 \, dx + \alpha \int_\Omega |\nabla u(x)| \, dx \quad (8)$$

$$E_2(b; I, u) = \int_\Omega (I(x) - u(x) - b(x))^2 \, dx + \beta \int_\Omega |\nabla b(x)|^2 \, dx \quad (9)$$

The energy minimization is performed by solving the associated Euler-Lagrange equations given by:

$$0 = \alpha \mathrm{div}\left(\frac{\nabla u(x)}{|\nabla u(x)|}\right) + 2\,(I(x) - u(x) - b(x)) \quad (10)$$

$$0 = \beta \Delta b(x) + (I(x) - u(x) - b(x)) \quad (11)$$

where the Neumann boundary condition is applied on $\partial\Omega$. An efficient ROF numerical scheme[39] is used for solving Eq. (10) and a fast conjugate gradient scheme is used for solving Eq. (11). Figure 2 shows the result of decomposition algorithm of the original MR images.

3.3. Interactive Segmentation

We propose an interactive image segmentation procedure that is performed based on the extraction of isocontour at a given point provided with a user interaction. A segmentation result is obtained by a sub-domain $D \subset \Omega$ confined by an isocontour that delineates the region boundary ∂D. The isocontour C_p at point $p \in \Omega$ on image u is defined by a simply connected closed curve of a constant intensity as follows:

$$C_p = \{x \mid u(x) = u(p), x \sim p\} \quad (12)$$

where $x \sim p$ indicates that x is connected to p along the curve C_p. For the extraction of isocontours, a modified marching cube algorithm[5] that propagates the curve from a specified point is used. The curve represents iso-value in the image by applying bilinear interpolation. The marching cube algorithm is aimed to trace contours at a certain constant intensity. The algorithm proceeds to examine the connectivity of the contour based on 8-neighborhood and extract contour segment using 16 possible segment configurations. A conventional marching cube algorithm requires a threshold value that is applied to global image domain,

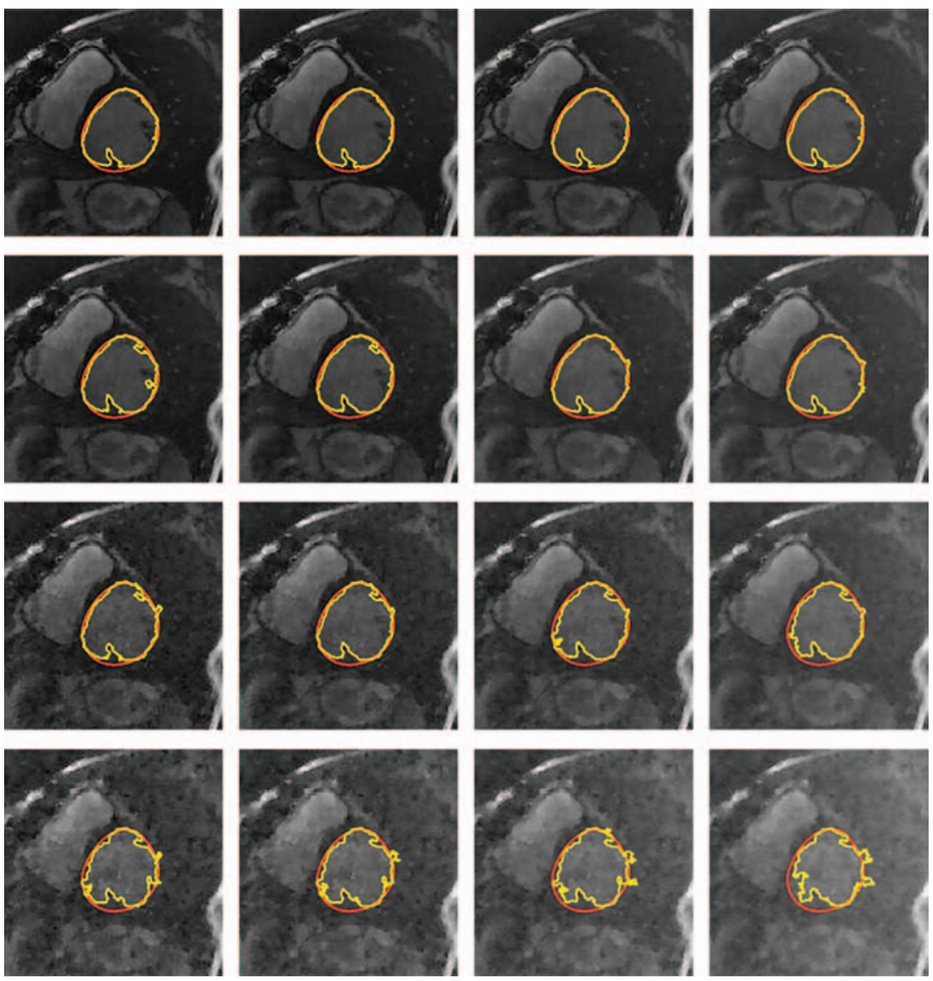

Fig. 6. The segmentation results for the left ventricle obtained from our intrinsic images that are computed from the images shown in Figure 5. The degree of noise is increased from top to bottom and the degree of bias field is increased from left to right. The segmentation results are shown in yellow color and the ground truth is shown in red color.

however our modified marching cube algorithm takes an initial point where the extraction of contour segment begins. In the procedure of the contour extraction, the algorithm interpolates exact points on the line connecting two neighboring points and moves to draw next contour segment. The algorithm sequentially draws line segments finding intensity values which are the same as the intensity value of the initial point. The terminal condition of the algorithm is that the current point is the same as the initial point forming a Jordan curve that refers to a simply closed curve. Our segmentation procedure builds on the fact that the intensity in medical imageries is derived from the relation between the physical properties of parts and their responses to the imaging source, which implies that the intensity of an image region corresponding to the same physical density is likely to be homogeneous.[41] However, this homogeneity assumption does not hold in the presence of bias fields, thus we apply the isocontour algorithm on the intrinsic representation obtained by our image decomposition scheme.

4. EXPERIMENTAL RESULTS

The performance of the proposed algorithm is evaluated by the segmentation of left ventricle in the MICCAI cardiac MRI dataset from which we choose cases with 64 largest left ventricle areas. In order to demonstrate the robustness of our segmentation algorithm for left ventricle in cardiac MRI images under undesirable bias field and noise, we build two datasets that are obtained by adding Gaussian noises and artificial linearly varying bias fields with different degrees. The dataset with artificial noises are generated by adding Gaussian noise with the standard deviation 0.1, 0.2, 0.4, and 0.8 to the original images and the example images with varying degrees of noise are presented on the first column in Figure 3 where the first image is an original one. The dataset with artificial bias fields are generated by adding the normalized linear gradation function ranged from 0 to 1 with multiplicative degree factors 0.1, 0.2, 0.4, and 0.8 to the example images with varying degrees of bias fields are presented on the first column in Figure 4 where the first image is an original one. In Figures 3 and 4, the image decomposition results are presented on the second column for the noise component, the third column for the bias field component, and the fourth column for the intrinsic image component. The visual illustration of the image decomposition results indicate that noises and bias fields at different levels are effectively segregated from the input images. The obtained intrinsic components are shown to be robust to represent the anatomical property of the organs. And the intrinsic representation based on the intrinsic component obtained by the image decomposition procedure, the segmentation of left ventricle is performed using an interactive isocontour algorithm with the manual selection of initial point. The selection of initial point in the extraction of isocontour is optimized with respect to the accuracy measured by the harmonic mean of precision and recall, which is called F-measure. In Figure 5, the segmentation results are obtained from the images with both noises and uneven bias fields at different levels demonstrating that the segmentation accuracy is highly degraded by noises and bias fields. The robustness of our segmentation algorithm with respect to noise and bias field is demonstrated in Figure 6 where the boundary of left ventricle is accurately obtained. As shown in the results, the accuracy of the left ventricle segmentation obtained from the images with noise or bias field is severely degraded as the degree of noise or bias field increases. On the other hand, the accuracy of the left ventricle segmentation obtained from the intrinsic images is precise despite largely corrupted image quality. The ground truth for the boundary of left ventricle is obtained by experienced cardiologists following the convention that includes papillary muscles and endocardial trabeculations in the ventricular cavity. The double blind annotation is employed to achieve better accuracy in defining the boundary of regions of interest. In Figures 5 and 6, the ground truth is presented in red curves for the quantitative evaluation of our segmentation results.

For the quantitative evaluation of the performance of our proposed algorithm, the accuracy measured by F-measure in the determination of the left ventricle boundary on the images with noise or bias field at different levels is presented in Figure 7 where the segmentation accuracy obtained from our intrinsic images outperforms the segmentation accuracy obtained from the original images. As the degree of noise or bias increases, the F-measure of original image which has noise and bias field decrease substantially. However, the F-measure of decomposed image with our proposed algorithm fairly maintains highly its value while increasing degree of noise and bias. As an additional measure for the quantitative evaluation, we present Dice measure that is computed by the area ratio of the union and the

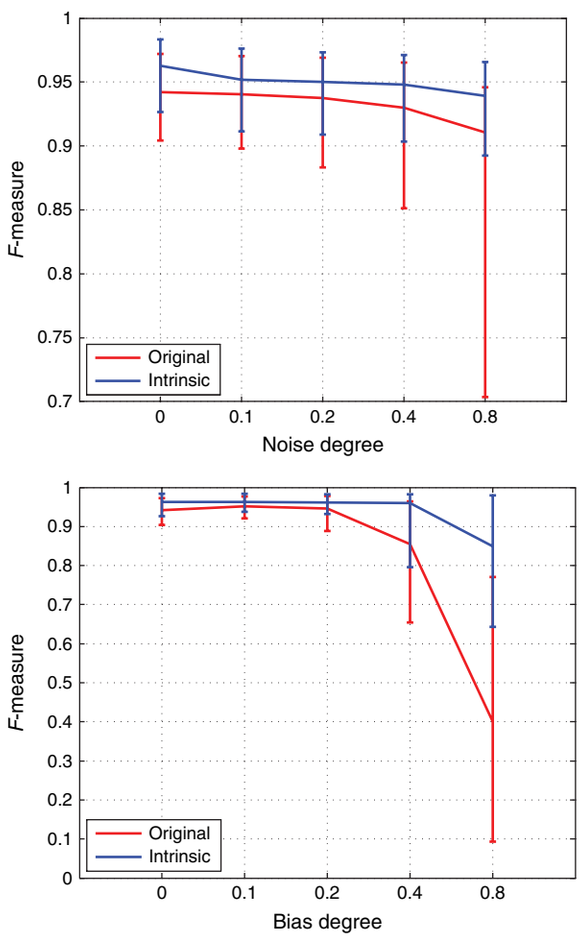

Fig. 7. Evaluation of the segmentation results obtained by optimal isocontours for the left ventricle from the original cardiac MRI and our intrinsic image with varying degrees of noise and bias field.

Table I. Quantitative evaluation of the segmentation results for the detection of left ventricle based on Dice measure from the cardiac images with varying degree of noise.

Noise degree	0.1	0.2	0.4	0.8
Original image	0.869 ± 0.129	0.794 ± 0.178	0.694 ± 0.211	0.478 ± 0.197
Intrinsic image	0.937 ± 0.031	0.928 ± 0.036	0.894 ± 0.079	0.800 ± 0.183

Table II. Quantitative evaluation of the segmentation results for the detection of left ventricle based on Dice measure from the cardiac images with varying degree of bias field.

Bias degree	0.1	0.2	0.4	0.8
Original image	0.934 ± 0.035	0.942 ± 0.027	0.935 ± 0.031	0.773 ± 0.144
Intrinsic image	0.942 ± 0.025	0.942 ± 0.026	0.943 ± 0.027	0.942 ± 0.028

intersection between the ground truth and the segmented region. The quantitative evaluations based on Dice measure are presented in Tables I and II for the segmentation accuracy of left ventricle from images with varying noise levels and with varying degrees of artificial bias fields.

5. CONCLUSIONS AND DISCUSSION

We have proposed an interactive segmentation algorithm for the left ventricle in cardiac MRI images using the isocontour algorithm from a specified point on the intrinsic representation obtained by our decomposition algorithm. Though there are some noise and bias field, our decomposition algorithm divide intrinsic image, noise, and bias field well. The intrinsic image performs better than contaminated image that has noise and bias field in the real clinical cases though we were using simple interactive segmentation algorithm. It has been reported that the Rician distribution is more realistic model for noise in MRI data, but we have assumed an additive Gaussian noise in our image model for computation simplicity. We have empirically demonstrated the robustness and effectiveness of our intrinsic representation derived from our simple image model in the delineation of the boundary of left ventricle from real cardiac MRI data. It has been shown that our intrinsic representation is effective in the delineation of regions of interest in cardiac MRI by a simple isocontour algorithm, and our algorithm is of great potential as the basis for an efficient and effective image annotation tool.

Acknowledgments: This Research was supported by the Chung-Ang University Excellent Student Scholarship and by NRF-2010-220-D00078, NRF-2011-0007898, and Converging Research Center Program, Ministry of Science, ICT and Future Planning (2013K000423), Korea.

References and Notes

1. K. K. L. Wong, R. M. Kelso, S. G. Worthley, P. Sanders, J. Mazumdar, and D. Abbott, Noninvasive cardiac flow assessment using high speed magnetic resonance fluid motion tracking. *Plos One* 4, e5688 **(2009)**.
2. K. K. L. Wong, R. M. Kelso, S. G. Worthley, P. Sanders, J. Mazumdar, and D. Abbott, Cardiac flow analysis applied to phase contrast magnetic resonance imaging of the heart. *Annals of Biomedical Engineering* 37, 1495 **(2009)**.
3. C. Pluempitiwiriyawej, J. M. F. Moura, Y.-J. L. Wu, and C. Ho, Stacs: New active contour scheme for cardiac mr image segmentation. *Medical Imaging, IEEE Transactions on* 24, 593 **(2005)**.
4. L. I. Rudin, S. Osher, and E. Fatemi, Nonlinear total variation based noise removal algorithms. *Physica D: Nonlinear Phenomena* 60, 259 **(1992)**.
5. W. E. Lorensen and H. E. Cline, Marching cubes: A high resolution 3d surface construction algorithm. *Computer Graphics* 21 **(1987)**.
6. D. Kang, J. Woo, P. J. Slomka, D. Dey, G. Germano, and C.-C. J. Kuo, Heart chambers and whole heart segmentation techniques: Review. *Journal of Electronic Imaging* 21, 010901–1 **(2012)**.
7. N. Senthilkumaran and R. Rajesh, Edge detection techniques for image segmentation—A survey, *Proc. Int. Conf. MSGSA* **(2008)**.
8. C. Pluempitiwiriyawej, J. M. F. Moura, Y.-J. L. Wu, and C. Ho, Stacs: New active contour scheme for cardiac mr image segmentation. *Medical Imaging, IEEE Transactions on* 24, 593 **(2005)**.
9. C. D. Garson, B. Li, S. T. Acton, and J. A. Hossack, Guiding automated left ventricular chamber segmentation in cardiac imaging using the concept of conserved myocardial volume. *Computerized Medical Imaging and Graphics* 32, 321 **(2008)**.
10. N. Paragios, A variational approach for the segmentation of the left ventricle in cardiac image analysis. *International Journal of Computer Vision* 50, 345 **(2002)**.
11. F. Billet, M. Sermesant, H. Delingette, and N. Ayache, Cardiac Motion Recovery and Boundary Conditions Estimation by Coupling an Electromechanical Model and Cine-MRI Data, Springer **(2009)**, pp. 376–385.
12. I. B. Ayed, S. Li, and I. Ross, Embedding overlap priors in variational left ventricle tracking. *Medical Imaging, IEEE Transactions on* 28, 1902 **(2009)**.
13. M. Lynch, O. Ghita, and P. F. Whelan, Segmentation of the left ventricle of the heart in 3-$d+t$ mri data using an optimized nonrigid temporal model. *Medical Imaging, IEEE Transactions on* 27, 195 **(2008)**.
14. K. K. L. Wong, R. M. Kelso, S. G. Worthley, P. Sanders, J. Mazumdar, and D. Abbott, Medical imaging and processing methods for cardiac flow reconstruction. *Journal of Mechanics in Medicine and Biology* 9, 1 **(2009)**.
15. K. K. L. Wong, Z. Sun, J. Tu, S. G. Worthley, J. Mazumdar, and D. Abbott, Medical image diagnostics based on computer-aided flow analysis using magnetic resonance images. *Computerized Medical Imaging and Graphics* 36, 527 **(2009)**.
16. T. F. Chan and L. A. Vese, Active contours without edges. *Image Processing, IEEE Transactions on* 10, 266 **(2001)**.
17. N. Paragios, A level set approach for shape-driven segmentation and tracking of the left ventricle, *Medical Imaging, IEEE Transactions on* 22, 773 **(2003)**.
18. M. Khare and R. K. Srivastava, Level set method for segmentation of medical images without reinitialization. *Journal of Medical Imaging and Health Informatics* 2, 158 **(2012)**.
19. E. A. Zanaty, A modified watershed transformation for distorted brain tissue segmentation. *Journal of Medical Imaging and Health Informatics* 2, 393 **(2012)**.
20. H. N. Lim, M. Y. Mashor, and R. Hassan, White blood cell segmentation for acute leukemia bone marrow images. *Biomedical Engineering (ICoBE), International Conference on*, IEEE **(2012)**, pp. 357–361.
21. K. K. L. Wong, J. Tu, Z. Sun, and D. W. Dissanayake, Methods in Research and Development of Biomedical Devices, World Scientific **(2013)**.
22. J. Cousty, L. Najman, M. Couprie, S. C.-Guinaudeau, T. Goissen, and J. Garot, Segmentation of 4d cardiac mri: Automated method based on spatio-temporal watershed cuts. *Image and Vision Computing* 28, 1229 **(2010)**.
23. M. Lynch, O. Ghita, and P. F. Whelan, Automatic segmentation of the left ventricle cavity and myocardium in mri data. *Computers in Biology and Medicine* 36, 389 **(2006)**.
24. C. A. Cocosco, W. J. Niessen, T. Netsch, E. Vonken, G. Lund, A. Stork, and M. A. Viergever, Automatic imagedriven segmentation of the ventricles in cardiac cine mri. *Journal of Magnetic Resonance Imaging* 28, 366 **(2008)**.
25. Y. Boykov and G. Funka-Lea, Graph cuts and efficient *n-d* image segmentation. *International Journal of Computer Vision* 70, 109 **(2006)**.
26. Y. T. Weldeselassie and G. Hamarneh, Dt-mri segmentation using graph cuts. *Medical Imaging*, International Society for Optics and Photonics, pp. 65121K–65121K–9.
27. M.-P. Jolly, Automatic segmentation of the left ventricle in cardiac mr and ct images. *International Journal of Computer Vision* 70, 151 **(2006)**.
28. X. Alb, F. I. Ventura, M. Rosa, K. Lekadir, C. T. Gomez, C. Hoogendoorn, and A. F. Frangi, Automatic cardiac lv segmentation in mri using modified graph cuts with smoothness and interslice constraints. *Magnetic Resonance in Medicine* **(2013)**.
29. M. B. Stegmann and D. Pedersen, Bi-temporal 3d active appearance models with applications to unsupervised ejection fraction estimation. *Medical Imaging*, International Society for Optics and Photonics, pp. 336–350.
30. H. C. V. Assen, M. G. Danilouchkine, A. F. Frangi, S. Ords, J. J. M. Westenberg, J. H. C. Reiber, and P. F. B. Lelieveldt, Spasm: A 3d-asm for segmentation of sparse and arbitrarily oriented cardiac mri data. *Medical Image Analysis* 10, 286 **(2006)**.

31. M. Lorenzo-Valds, G. I. Sanchez-Ortiz, R. Mohiaddin, and D. Rueckert, Atlas-Based Segmentation and Tracking of 3D Cardiac MR Images Using Non-Rigid registration, Springer **(2002)**, pp. 642–650.

32. M. Lorenzo-Valds, G. I. Sanchez-Ortiz, A. G. Elkington, R. H. Mohiaddin, and D. Rueckert, Segmentation of 4d cardiac mr images using a probabilistic atlas and the em algorithm. *Medical Image Analysis* 8, 255 **(2004)**.

33. X. Zhuang, D. J. Hawkes, W. R. Crum, R. Boubertakh, S. Uribe, D. Atkinson, P. Batchelor, T. Schaeffter, R. Razavi, and D. L. G. Hill, Robust registration between cardiac mri images and atlas for segmentation propagation. *Medical Imaging*, International Society for Optics and Photonics, pp. 691408–691408–11.

34. M. Lynch, O. Ghita, and P. F. Whelan, Left-ventricle myocardium segmentation using a coupled level-set with a priori knowledge. *Computerized Medical Imaging and Graphics* 30, 255 **(2006)**.

35. S. Zambal, J. Hladvka, and K. Bhler, Improving Segmentation of the Left Ventricle Using a Two-Component Statistical Model, Springer **(2006)**, pp. 151–158.

36. H. Zhang, A. Wahle, R. K. Johnson, T. D. Scholz, and M. Sonka, 4-d cardiac mr image analysis: Left and right ventricular morphology and function. *Medical Imaging, IEEE Transactions on* 29, 350 **(2010)**.

37. A. Simmons, P. S. Tofts, G. J. Barker, and S. R. Arridge, Sources of intensity nonuniformity in spin echo images at 1.5 t. *Magnetic Resonance in Medicine* 32, 121 **(1994)**.

38. A. Sawatzky, D. Tenbrinck, X. Jiang, and M. Burger, A variational framework for region-based segmentation incorporating physical noise models. *Journal of Mathematical Imaging and Vision* 1 **(2012)**.

39. L. I. Rudin, S. Osher, and E. Fatemi, Nonlinear total variation based noise removal algorithms. *Physica D: Nonlinear Phenomena* **(1992)**.

40. W. H. Fleming and R. Rishel, An integral formula for the total gradient variation. *Archiv der Mathematik* 11, 218 **(1960)**.

41. S. Wijewickrema, I. Ioannou, and G. Kennedy, Adaptation of marching cubes for the simulation of material removal from segmented volume data. *Computer-Based Medical Systems (CBMS), 2013 IEEE 26th International Symposium on*, June **(2013)**, pp. 29–34.

Received: 8 January 2014. Accepted: 1 March 2014.